A Comparison of Linear Periodic and Nonlinear Control Strategies for Self-Sensing Magnetic Bearings

Raoul Herzog[1,a], Philippe Blanc[1,b]
HEIG–VD, CH–1400 Yverdon
[1]HES–SO, University of Applied Sciences Western Switzerland
[a]raoul.herzog@heig–vd.ch, [b]philippe.blanc@heig–vd.ch

Abstract: In this paper, the controller design for self–sensing magnetic bearings is considered using a linear time periodic (LTP) framework. The time periodicity comes from a deliberate bias flux excitation signal allowing to improve the plant properties. Design trade–offs using periodic controllers are investigated. Three design objectives are considered: 1) low sensitivity norm to ensure good robustness, 2) low controller gain to attenuate current measurement noise and to avoid voltage saturation, and 3) low mechanical compliance against external perturbation forces to ensure high bearing stiffness. Different LTP H_∞ controllers are designed using lifting techniques and linear matrix inequalities (LMI). The resulting controllers are validated using closed–loop simulations with the nonlinear plant.

Keywords: Self–Sensing, Linear Time Periodic Systems (LTP), Periodic H_∞ Control

Introduction

Self–sensing permits active magnetic bearings to dispense with dedicated position sensors and, instead, reconstruct rotor position information from the voltage and current signals of the actuator coils. Thus, the hardware amount in the machine environment and the amount of cabling can be reduced, which potentially increases hardware reliability.
But all experts in magnetic bearings agree that self–sensing is inherently difficult, and may potentially suffer from poor performance and/or poor robustness. The research activities in self–sensing were boosted with the announcement of the first commercial self–sensing magnetic bearing for turbomolecular pumps [1] and with the publication of [2], [3] opening new research directions in self–sensing. In [2] the achievable robustness of self–sensing is analyzed in a linear periodic (LTP) framework. It is concluded that the achievable robustness dramatically improves by exciting the system with a periodic flux signal (dither) and by utilizing linear time periodic controllers. The cur-rent paper continues and extends the research direction of [2] and [4]. This paper has two objectives:

- to analyze the achievable performance and robustness in the case of low dither frequency. This is important to avoid the sensitivity deteriorating effects of eddy currents, and to be more independent from parasitic capacitance (e.g. long bearing cables). Dither frequencies in the range of 4... 20 times higher than the closed–loop bandwidth are considered. Synchronous demodulation allows to build a special case of periodic controllers, but they typically need a much higher gap between the bandwidth and the dither frequency.
- to analyze and compare in simulation the robustness and performance of several linear peri-odic and nonlinear estimator and control strategies for self–sensing magnetic bearings. Multi–objective design trade–offs between robustness, noise attenuation and bearing stiffness are investigated.

2 Modelling

2.1 Standard Nonlinear Model

The following simplification hypotheses are assumed throughout this chapter: eddy currents, leakage and fringing effects are neglected, the magnetic material is assumed to be linear (no saturation, no hysteresis), and the flux density is assumed to be uniformly distributed throughout the magnet core and air gap. The modelling used in this paper is standard and corresponds to [2]. Ampère's law gives the following relation between the magnetic fluxes Φ_i in each magnet and the coil currents I_i:

$$\Phi_1 = \frac{\mu_0 A_g N}{2(g_0 + x_g)} I_1 \quad , \quad \Phi_2 = \frac{\mu_0 A_g N}{2(g_0 - x_g)} I_2. \tag{1}$$

Here, μ_0 denotes the permeability of free space, N is the number of coil turns on each magnet, A denotes the gap area under each magnet, and g_0 is the nominal air gap on each side when the rotor is centered. In (1), the iron length l_{fe} is either neglected or subsumed into the nominal gap $g_0 = g_{0,air} + l_{\text{fe}}/\mu_r$. Combining the Kirchhoff law with Faraday's induction law yields

$$U_1 = N\frac{d\Phi_1}{dt} + R\, I_1 \quad , \quad U_2 = N\frac{d\Phi_2}{dt} + R\, I_2 \tag{2}$$

in which R is the ohmic coil resistance, U_i are the voltages applied to the coils (input signals), and I_i are the measured coil currents (output signals). The principle of virtual work allows to determine the attractive forces f_1, f_2 produced by each electromagnet. They are given by

$$f_1 = \frac{\Phi_1^2}{\mu_0 A_g} \quad , \quad f_2 = \frac{\Phi_2^2}{\mu_0 A_g}. \tag{3}$$

Newton's law leads to

$$m\,\frac{d^2 x_g}{dt^2} = \frac{\Phi_2^2 - \Phi_1^2}{\mu_0 A_g} + f_{ext} \tag{4}$$

where m is the rotor mass and f_{ext} is an unknown disturbance force. Equation (1) and (2) lead to

$$\frac{d\Phi_1}{dt} = -R\,\frac{2(g_0 + x_g)}{\mu_0 A_g N^2}\,\Phi_1 + \frac{U_1}{N} \quad , \quad \frac{d\Phi_2}{dt} = -R\,\frac{2(g_0 - x_g)}{\mu_0 A_g N^2}\,\Phi_2 + \frac{U_2}{N}. \tag{5}$$

Equations (4), (5) and (1) form a 4th order nonlinear model with input U_1, U_2 and output I_1 and I_2.

2.2 Scaling and Variable Change

Scaling the state variables and the time axis has several benefits: the number of parameters is reduced allowing a deeper physical insight, and the order of magnitude of all scaled state variables is close to one. This improves the numerical conditionning of the subsequent LMI optimization problem. Following [2] the normalization is based on the saturation[1] flux density of the material B_{sat}. The time scale can be normalized by $\tilde{t} = t/\tau_m$, where τ_m is an electro–mechanical time constant. The latter corresponds to the minimum time of flight of mass m from center to contact with one of the magnets applying maximum force corresponding to saturation B_{sat}. Additionally, a variable change in the state, input and output variables is applied which replaces the individual signals of both actuators $(\cdot)_1, (\cdot)_2$ by the sum and the difference signals denoted with subscripts $(\cdot)_s, (\cdot)_d$.

[1] The choice of B_{sat} has no effect on the subsequent results because it just rescales the internal states of the model.

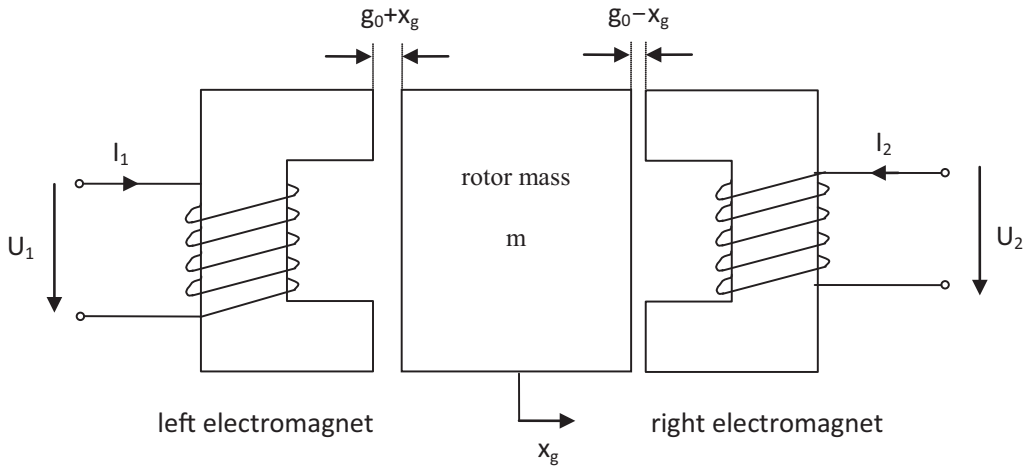

Figure 1: Magnetic Bearing Configuration.

The only remaining parameter of the scaled plant is time scale ratio $\eta = \tau_m/\tau_e$, where τ_e denotes the electrical time scale $\tau_e = L_0/R$. Following [2] we get the non–dimensional system (S)

$$\begin{aligned} \dot{x}_n &= v && (6)\\ \dot{v} &= \phi_s\,\phi_d && (7)\\ \dot{\phi}_d &= -\eta\,\phi_d + \eta\,x_n\,\phi_s + u_d && (8)\\ \dot{\phi}_s &= -\eta\,\phi_s + \eta\,x_n\,\phi_d + u_s && (9)\\ i_d &= \phi_d - x_n\,\phi_s && (10)\\ i_s &= \phi_s - x_n\,\phi_d && (11) \end{aligned}$$

where the derivation dot $\dot{}$ means $d/d\tilde{t}$. For the ease of notation, the tilde is left away in the sequel and the normalized time is simply called t. The only nonlinearities appearing in the above model are the products[2] of state variables $x_n\,\phi_s$ and $x_n\,\phi_d$. If we could impose the bias flux signal $\phi_s(t)$ the system would become *linear* with *time varying* coefficients. The following chapter shows how this can be achieved approximately.

2.3 Linearization and System Decoupling

We linearize the above system around a periodic trajectory for the case without load $f_{ext} = 0$. For this we fix a periodic signal $u_s(t)$ and denote by $\phi_{sp}(t)$ the unique periodic solution of equation $\dot{\phi}_s = -\eta\,\phi_s + u_s$. Assuming $u_d = 0$, one observes that $x = (0, 0, 0, \phi_{sp})^t$ is a periodic solution of system (S). A linearization around this solution leads to a decoupled system which consists of a first order LTI system for the state ϕ_s and a third order LTP for the states x_n, v, ϕ_d, see figure 2. The latter is given by

$$\begin{pmatrix} \dot{x}_n \\ \dot{v} \\ \dot{\phi}_d \end{pmatrix} = \begin{pmatrix} 0 & 1 & 0 \\ 0 & 0 & \phi_{sp}(t) \\ \eta\,\phi_{sp}(t) & 0 & -\eta \end{pmatrix} \begin{pmatrix} x_n \\ v \\ \phi_d \end{pmatrix} + \begin{pmatrix} 0 \\ 0 \\ 1 \end{pmatrix} u_d \qquad (12)$$

$$i_d = \begin{pmatrix} -\phi_{sp}(t) & 0 & 1 \end{pmatrix} \begin{pmatrix} x_n \\ v \\ \phi_d \end{pmatrix}. \qquad (13)$$

In the following, signal $u_s(t)$ will be chosen in order that $\phi_{sp}(t) = \phi_0\,(1 + \Gamma_{\text{ext}}\,\sin(\omega_{\text{ext}}\,t))$.

[2] If the bias flux ϕ_s varies much faster than displacement x_n the product $x_n\,\phi_s$ causes a modulation of current i_d in (10).

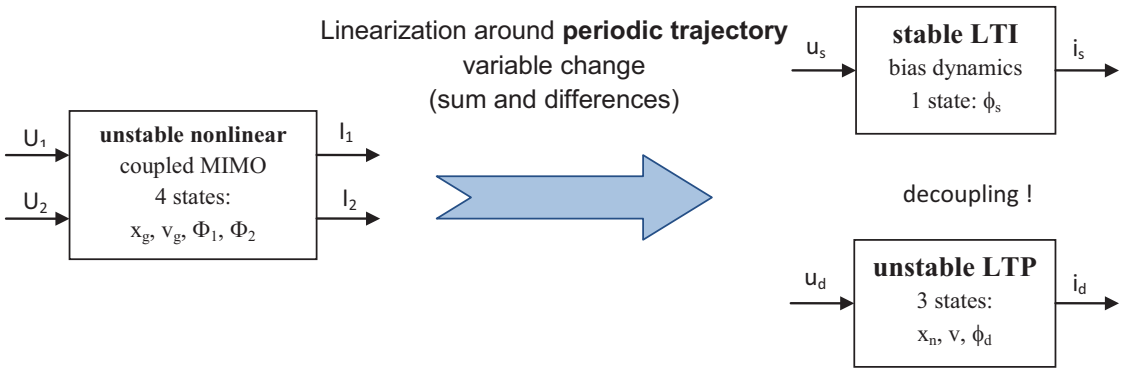

Figure 2: Linearization around periodic trajectory leads to decoupling.

2.4 Discretization and Lifting

Following [4] the LTP model can be discretized using an Euler approximation at the sampling rate $t_s = 2\pi/(N_p\,\omega_{\text{ext}})$, where N_p is the number of desired sample points over one period. This yields a discrete periodic system of the form

$$x(k+1) = A(k)\,x(k) + B\,u_d(k) \tag{14}$$
$$y(k) = i_d(k) = C(k)\,x(k) \tag{15}$$

where $A(k)$ and $C(k)$ are varying with period N_p, i.e. $A(k+N_p) = A(k)$ and $C(k+N_p) = C(k)$. The theory for tackling such linear periodic systems is well developed, refer to [5, 6]. A particularly useful norm–preserving lifting technique [6] allows to transform the discretized LTP plant into a multivariable LTI plant. The input and output signals over one period are packed into vector signals, and the system is resampled at period $T_p = 2\pi/\omega_{\text{ext}}$. This allows to benefit from the huge panoply of existing LTI tools.

Table 1: Physical and non–dimensional parameters

	symbol	value	unit
max. current	I_{max}	3	A
max. voltage	U_{max}	100	V
number of turns	N	180	-
nominal air gap	g_0	0.55	mm
mean pole area	A_g	604	mm^2
coil resistance at DC	R	3.0	Ω
nominal inductance @ g_0=0.55 mm	L_0	22.35	mH
rotor mass	m	3.31	kg
bias current	I_0	1.5	A
magnetic saturation scaling	B_{sat}	1.2	T
mechanical time constant	τ_m	$1.6218 \cdot 10^{-3}$	s
electrical time constant	τ_e	$7.4521 \cdot 10^{-3}$	s
ratio of time scales	η	0.2176	-
nondimensional bias flux	Φ_0	0.6169	-

3 Problem Setup for LTP Controller Synthesis

A first result concerns the analysis of achievable robustness for low frequency dither excitation. As robustness measure the norm of the input sensitivity[3] $||S_i||_\infty = ||(I - C\,P)^{-1}||_\infty$ is used, where P denotes the LTP plant and C denotes the LTP controller. Table 1 lists the parameter values used for the following study. Figure 3 shows the achievable input sensitivity norm as a function of excitation amplitude Γ_{ext} for two different excitation frequencies ω_{ext}. It appears that the bounds [2, 4] are too optimistic, and that the achievable input sensitivity norm is *not* monotonically decreasing w.r.t. excitation amplitude Γ_{exc}. As a worrying result, it appears that *low excitation frequencies and low excitation amplitudes* may behave *worse* than no excitation at all!

The discrepancy with [2, 4] can be explained as follows: the lifted LTI state–space matrices have a specific structure resulting from the lifting process. The feedthrough matrix D has a triangular structure resulting from the causality of the underlying LTP plant. When optimizing over all stabilizing LTI controllers in the lifted space, the structural constraints are *not* taken into account, and the bounds are too optimistic. Furthermore, delifting of the resulting controller is impossible. As a remedy, the present work uses direct LTP synthesis using periodic Riccati equations [6] and linear matrix inequalities (LMI). The latter approach is available as LTV toolbox [7].

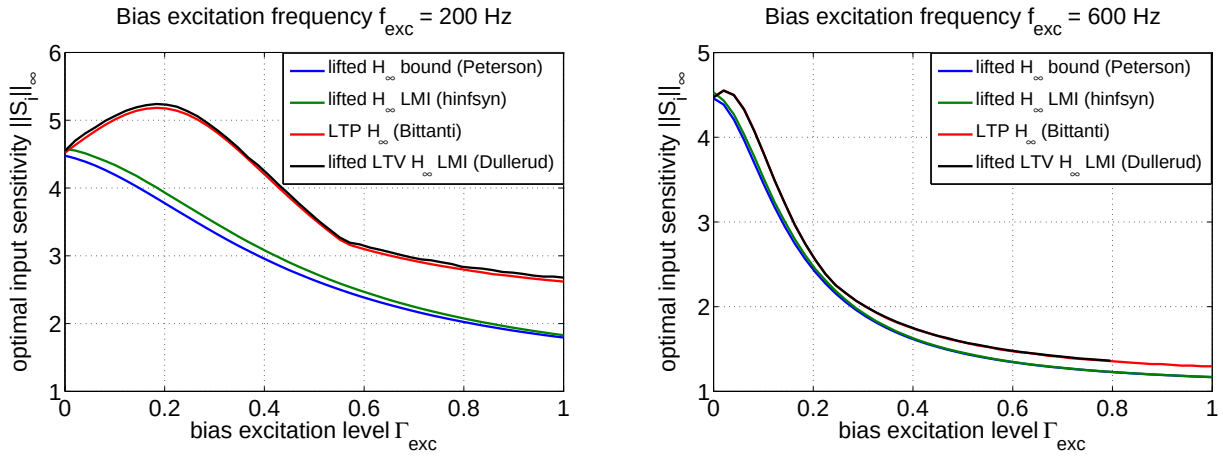

Figure 3: Achievable robustness as a function of dither excitation amplitude and frequency.

Minimizing the sensitivity norm is an ill–posed problem since the resulting controller has infinite high frequency gain. Therefore, a multi–objective design problem is formulated according to figure 4. Two exogenous performance channels are introduced. The first channel goes from $(w_1, w_2)^t$ to z_1 leading to the closed–loop map $((I - C\,P)^{-1},\ (I - C\,P)^{-1}\,C\,W_c)$. Here, W_c is a scalar weighting allowing to penalize the high frequency controller gain. The second channel goes from w_3 to z_2 leading to a closed–loop map $W_{f2}\,T_c\,W_{f1}$. Here, T_c represents the map from an external disturbance force to the rotor displacement subsequently called mechanical compliance. The scalar weightings W_{f1} and W_{f2} allow to penalize the norm of mechanical compliance T_c. The spatial constraint given by the channel structure is captured by the square norm [7]. The corresponding design problem is *convex* and can be solved by LMI's using the LTV toolbox [7]. For $N_p = 50$ points per period the resulting LMI problem turns out to have almost 1'000 scalar decision variables. The calculation takes about 5 minutes on a standard PC. It makes no sense to choose a higher value of N_p since the result is almost independent from N_p beyond $N_p > 50$. Furthermore, numerical problems may occur if N_p is too high, and the calculation time increases rapidly.

[3]The ISO standard (14839-3) for AMB systems recommends a threshold sensitivity of 3.0 for the acceptance of commercial AMB systems. This value is based on consensus of industry experts.

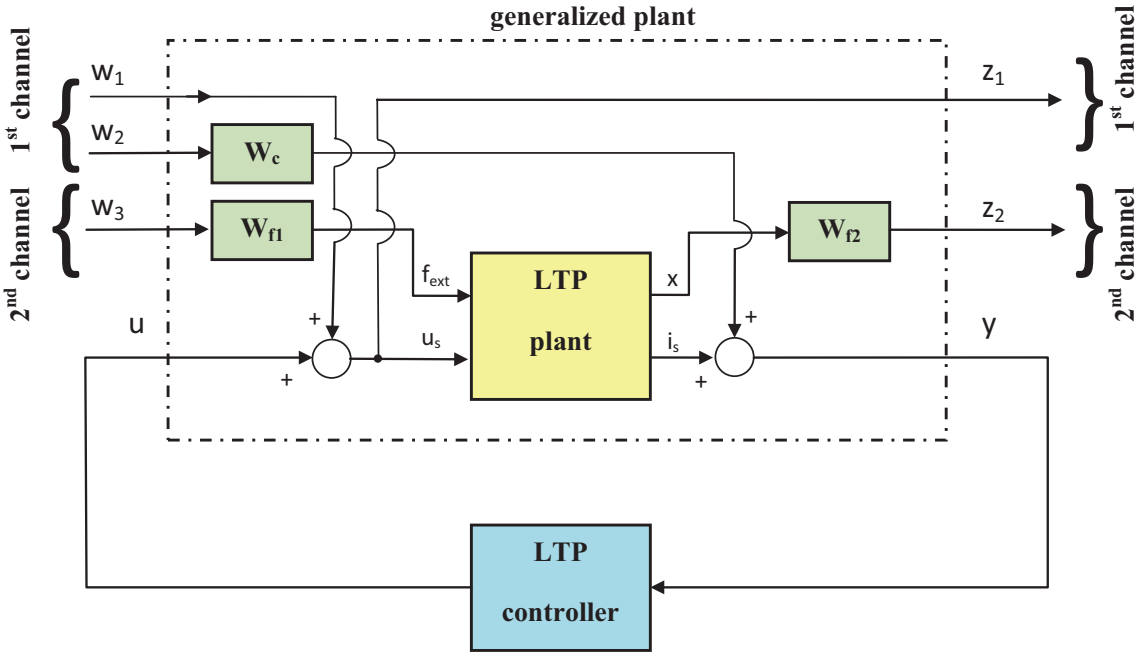

Figure 4: Problem setup for LTP $\mathcal{H}_\infty$ optimization.

4 LTP Controller Results

The resulting closed–loop of LTP controller and linearized LTP plant is analyzed. The closed–loop matrices are found by lifting the LTP plant and the LTP controller to discrete LTI systems, and by building the feedback interconnection.

Table 2: Performance trade–offs for different excitation and weighting parameters

trial	f_{exc} Hz	Γ_{exc}	N_p	W_c	W_{f1}	W_{f2}	$\|\|S_i\|\|_\infty$	$\|\|C\|\|_\infty$ V/A	$\|\|T_c\|\|_\infty$ μm/N	comment
1#	0	-	-	0.0	0.0	0.0	4.45	∞	7.5	LTI, opt. sensitivity bound
2#	0	-	-	0.3	0.0	0.0	4.85	218	8.4	LTI, mixed sensitivity
3#	200	0.5	50	0.1	0.0	0.0	3.61	3'169	19.1	LTP, high controller gain
4#	200	0.5	50	0.3	0.0	0.0	3.88	425	18.0	reduced controller gain
5#	200	0.5	30	0.3	0.0	0.0	3.91	414	18.1	quite insensitive w.r.t. N
6#	400	0.5	30	0.2	0.0	0.0	2.15	474	24.0	mech. compliance too high
7#	400	0.5	30	0.2	1.0	0.2	3.84	834	8.3	compl. $\searrow$, but otherwise ...
8#	1000	0.5	30	0.4	0.0	0.0	1.97	164	20	compliance too high
9#	1000	0.5	30	0.4	1.0	0.2	2.91	262	7.5	better compliance
10#	1000	0.2	30	0.4	1.0	0.2	4.92	237	5.4	lower excitation level
11#	1000	0.2	30	0.4	0.0	0.0	3.42	155	9.2	sensitivity $\searrow$

The virtual sampling period of the lifted closed–loop corresponds to $t_s = 1/f_{exc}$. The analysis carried out comprises the computation[4] of the closed–loop poles, the $\mathcal{H}_\infty$ norm of the input sensitivity $||S_i||_\infty$, the controller norm $||C||_\infty$, and the norm of mechanical compliance $||T_c||_\infty$.

[4]Using the Robust Control Toolbox of Mathworks©.

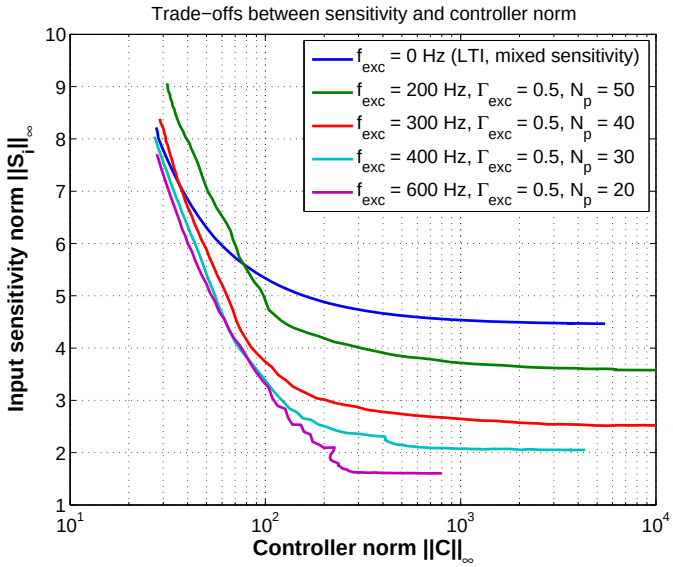

Figure 5: Possible Trade–Offs.

The discrete closed–loop poles in the z domain can be converted to equivalent s domain poles by the relationship $s = \log(z)/t_s$. It turns out that the closed–loop poles include the stable plant pole $s = -167 \pm 198\,j$ rad/s for the case without compliance weighting $W_{f1} = W_{f2} = 0$. This closed–loop pole is the slowest because its the closest pole w.r.t. the imaginary axis, and therefore becomes dominant for the transient behaviour. The corresponding undamped natural frequency corresponds to $f_{cl} = |s|/(2\,\pi) = 41$ Hz. For non–zero compliance weightings W_{f1}, W_{f2}, we observed that the natural frequency of the dominant closed–loop pole increases. For the case #9 of table 2, the dominant natural closed–loop frequency increases to $f_{cl} = 54$ Hz due to higher compliance weighting.

To analyze the results in table 2 we introduce the ratio f_{exc}/f_{cl}. The case $f_{exc} = 200$ Hz corresponds to an excitation ratio of $f_{exc}/f_{cl} \approx 5$.

For low excitation ratios $f_{exc}/f_{cl} < 5$ and low excitation levels $\Gamma_{exc} < 0.4$ the achievable robustness of the LTP system is *worse* than for the LTI case with no excitation since the curve of $||S_i||_\infty$ in figure 3 is not monotonically decreasing w.r.t. excitation amplitude Γ_{exc}. This result is new and surprising. Table 2 shows that a low excitation ratio of $f_{exc}/f_{cl} = 5$ and an excitation level of $\Gamma_{exc} = 0.5$ is not realistic because the input sensitivity norm and/or the controller norm are too high.

A realistic controller design needs an excitation ratio $f_{exc}/f_{cl} > 10$. This corresponds to the 400 Hz case in table 2 where moderate sensitivity and controller norms can be achieved. But the mechanical compliance stays high, which corresponds to *low bearing stiffness*. A high stiffness self–sensing bearing with acceptable robustness properties and realistic performance needs an excitation ratio $f_{exc}/f_{cl} > 20$. Design #9 in table 2 shows a trade–off where all of the three objectives yield acceptable values. However it should be noted that such high frequency excitations need enough voltage supply level (100V in case #9), and may violate the assumption of negligible eddy currents.

Figure 6 shows a closed–loop simulation using the LTP controller design #9 from table 2 and the original *nonlinear* plant. The bias excitation is injected via voltage u_s using the inverse dynamics of the LTI bias plant[5]. A perturbation force is applied as external excitation signal. This perturbation

[5]In practice, the value of coil resistance R is subject to thermal drift. Since this drift is very slow the precise value of R can

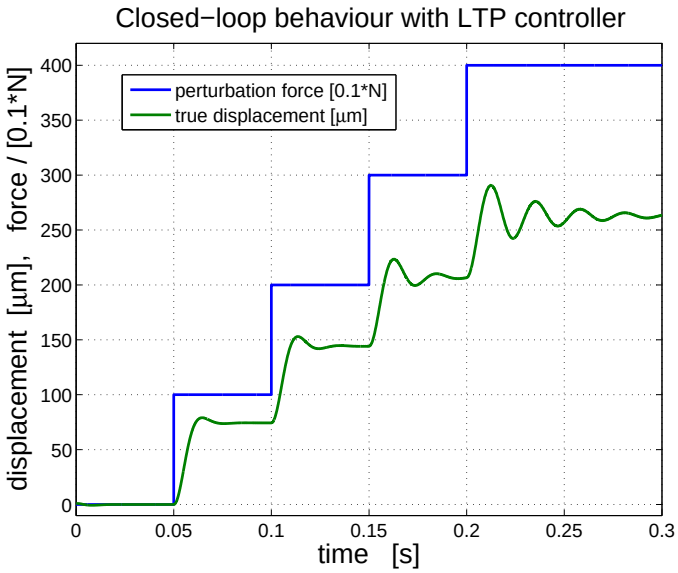

Figure 6: Closed–loop simulation result with nonlinear plant and LTP controller design #9.

force steps by increments of 10 N from zero to 40 N. The time response of the true displacement is shown in figure 6. The result shows a fast and well–damped behaviour of the displacement for the first two steps. Note that the controller does not exhibit an integral term which explains the static excursion of displacement. The static compliance and the norm $||T_c||_\infty$ have the same order of magnitude. For the high load steps from 20 to 30 N and from 30 to 40 N the damping of the time response progressively decreases. The final value of displacement corresponds to a typical value of rotor clearance (0.25 mm), which is usually half the value of the air gap (0.5 mm). The progressive change of the step response at high load is explained by the plant nonlinearity. The change is due to a change in bias flux $\phi_{sp}(t)$. The periodic trajectory no longer corresponds to the periodic trajectory used for linearization. The decoupling of the LTI bias dynamics and the LTP differential dynamics becomes non–ideal at high load conditions.

5 Nonlinear Controller Results

Extended (nonlinear) Kalman estimators (EKF) and the nonlinear Lyapunov–based Maslen estimator [3] have been investigated. The overall control structure comprises a cascade structure with a flux controller, and a position controller having the desired bearing force as output signal. This cascade structure is a special case of observer–based state feedback with time–periodic coefficients. For both nonlinear approaches parametrizations were found allowing a stable closed–loop. Compared to the LTP controller case it is much less obvious how to tune the parameters and how to find good design trade–offs. The lack of the panoply of analysis tools available for LTI and LTP systems impedes the search for good design trade–offs in the nonlinear case. The detailed results will be presented in a later publication.

6 Conclusion

The LTP $\mathcal{H}_\infty$ approach presented in this paper is a very systematic approach for investigating design trade–offs involving the sensitivity norm, the controller gain, and the resulting bearing compliance. It allows to generate a discrete linear time–periodic controller described by state–space matrices

easily be tracked by dividing averaged values of voltage and measured current.

$A_c(k),B_c(k),C_c(k),D_c(k)$ where the index k cyclically sweeps from 1 to N_p and back to 1. All matrices are pre–computed offline using LMI optimization techniques, and can be stored in target memory which allows a very efficient real–time implementation of the controller. It is shown that the ratio between the excitation frequency and the natural frequency of the dominant closed–loop pole should be higher than 20, i.e. $f_{exc}/f_{cl} > 20$ to ensure good robustness and performance properties.

7 Outlook

A magnetic bearing test rig is currently being developed in order to implement and experimentally validate the results obtained in this paper.

A certain number of open questions remains. A first question concerns the choice of input sensitivity norm as an indicator for robustness. Of course this choice was guided by the ISO standard 14839–3 stipulating a reasonable threshold sensitivity of 3.0. But the ISO standard concerns standard *sensor–based* magnetic bearings, and today, there is no available field experience indicating whether it is reasonable or not to apply the ISO standard to self–sensing bearings. Sensitivity norm optimization over the large class of LTP uncertainty operators may induce conservatism. It would be interesting to consider a more realistic polytopic model for parameter uncertainties.

Another important point concerns the inclusion of *eddy currents* in the model. It would be interesting to utilize the LTP framework described in this paper for the eddy current model, and to investigate the optimal choice of excitation frequency.

A last issue concerns *multi–objective* H_∞ control. Instead of using the spatial constraint method described in [5] it might be interesting to investigate the multi–objective approach proposed in [8].

Acknowledgements

This work was supported by the ‘réserve stratégique’ (Sage-X project 17922) of the University of Applied Sciences Western Switzerland (HES–SO). We would also like to thank Geir Dullerud for his valuable advices and for providing us with his LTV toolbox.

References

[1] M. Brunet. Self-sensing technology, simplified mechanical design. *S2M news no. 5*, dec 2005.

[2] Eric H. Maslen, Dominick T. Montie, and Tetsuya Iwasaki. Robustness limitations in self-sensing magnetic bearings. *ASME Journal of Dynamic Systems, Measurement, and Control*, 128:197–203, 2006.

[3] Eric H.Maslen, Tetsuya Iwasaki, and RozaMahmoodian. Formal parameter estimation for self–sensing. *Tenth International Symposium on Magnetic Bearing, ISMB10, Martigny, Switzerland*, 2006.

[4] K.S. Peterson, R.H. Middleton, and J.S. Freudenberg. Fundamental limitations in self–sensing magnetic bearings when modeled as linear periodic systems. *Proceedings of the American Controls Conference*, 2005.

[5] G.E. Dullerud and F. Paganini. A course in robust control theory. A convex approach. *Springer*, 2000.

[6] S. Bittanti and P. Colaneri. *Periodic Systems, Filtering and Control*. Springer book, 2009.

[7] G.E. Dullerud and S. Lall. A new approach for analysis and synthesis of time–varying systems. *IEEE Transactions on Automatic Control*, 44:1486–1497, 1999.

[8] Carsten Scherer, Pascal Gahinet, andMahmoud Chilali. Multiobjective output- feedback control via LMI optimization. *IEEE Transactions on Automatic Control*, 42:896–911, 1997.